generate CdS crystals. The background conductance of these junctions is well understood on the basis of the work of CDMT.[1] These tunnel junctions exhibit strong structure at biases corresponding to the LO phonon energy which may be understood, at least qualitatively, by consideration of the $E(k)$ relation in the semiconductor as modified by screened polar coupling to the LO phonon. The results are contrasted with existing data on GaAs junctions where the electron-phonon coupling is of the same type but considerably weaker.

Studies of the conductance peaks of the Appelbaum-Anderson type have shown that their magnetic field dependence is consistent with the model of Wolf and Losee[12] for the microscopic origin of the localized magnetic moments in a Schottky barrier. A large negative g shift is observed for these moments and lifetime broadening effects appear to be important in understanding the detailed structure of the ZBA.

ACKNOWLEDGMENTS

We wish to thank Dr. L. C. Davis for supplying a computer program for the CDMT calculation, and Dr. L. C. Davis and Dr. C. B. Duke for useful discussions and communication of the results of their calculations prior to publication. We wish to thank L. G. Rubin for technical assistance during our visit to the National Magnet Laboratory and Dr. B. C. Cavenett, Dr. R. P. Khosla, and Dr. D. C. Hoesterey for helpful discussions.

PHYSICAL REVIEW VOLUME 187, NUMBER 3 15 NOVEMBER 1969

Spectroscopic Investigation of Acceptor States in Aluminum Antimonide*

B. T. AHLBURN AND A. K. RAMDAS
Department of Physics, Purdue University, Lafayette, Indiana 47907
(Received 6 June 1969)

Photoexcitation spectra associated with acceptors in p-type aluminum antimonide have been studied. Four sets of sharp photoexcitation lines are observed at liquid-helium temperature; they are absent at liquid-nitrogen or higher temperatures. Equal spacings between pairs of prominent lines in three of these spectra are consistent with an effective-mass-like description for the excited states. The effect of uniaxial stress on several of the acceptor photoexcitation lines has been studied for compressive force **F** parallel to ⟨111⟩ or ⟨100⟩. The splittings and the polarization patterns may be interpreted if it is assumed that the acceptor centers have T_d site symmetry, and that the bound hole states are not sensitive to a possible departure from a germaniumlike valence band with its maximum at $\mathbf{k}=0$.

I. INTRODUCTION

ACCEPTOR centers can be formed in a III-V compound such as aluminum antimonide in a number of ways. For example, a group-II atom, when substituted for an aluminum atom in the aluminum antimonide lattice can act as an acceptor,[1] as can a group-IV atom substituted for an antimony atom.[1] More complicated acceptor centers, associated with vacancies, interstitial atoms, or clusters of impurities can also be visualized.

Extensive studies of donor and acceptor photoexcitation spectra in germanium[2,3] and silicon[4–6] have demonstrated that significant information about the states of charge carriers bound to the impurities and about properties of the host crystal can be obtained from such investigations. The application of uniaxial stress, used in conjunction with linearly polarized light, has proven to be of considerable value in interpreting these spectra.[4–9] Among the III-V compounds, photoexcitation spectra have been observed for tellurium and selenium donors in aluminum antimonide,[10] manganese acceptors in gallium arsenide,[11] and in n-type indium antimonide with the application of high magnetic fields.[12] Preliminary observations of acceptor spectra in gallium antimonide and indium antimonide have also been made.[13] The authors have presented brief reports[14] on the photoexcitation spectra of acceptors in aluminum

* Work supported by the Advanced Research Projects Agency.
[1] O. Madelung, *Physics of III–V Compounds* (John Wiley & Sons, Inc., New York, 1964), Chap. 5, p. 221.
[2] J. H. Reuszer and P. Fisher, Phys. Rev. **135**, A1125 (1964).
[3] R. L. Jones and P. Fisher, J. Phys. Chem. Solids **26**, 1125 (1965).
[4] R. L. Aggarwal and A. K. Ramdas, Phys. Rev. **137**, A602 (1965).
[5] R. L. Aggarwal and A. K. Ramdas, Phys. Rev. **140**, A1246 (1965).
[6] A. Onton, P. Fisher, and A. K. Ramdas, Phys. Rev. **163**, 686 (1967).
[7] R. L. Jones and P. Fisher, Solid State Commun. **2**, 369 (1964).
[8] J. H. Reuszer and P. Fisher, Phys. Rev. **140**, A245 (1965).
[9] D. H. Dickey and J. O. Dimmock, J. Phys. Chem. Solids **28**, 529 (1967).
[10] B. T. Ahlburn and A. K. Ramdas, Phys. Rev. **167**, 717 (1968).
[11] R. A. Chapman and W. G. Hutchinson, Phys. Rev. Letters **18**, 443 (1967).
[12] R. Kaplan, J. Phys. Soc. Japan Suppl. **21**, 249 (1966).
[13] P. Fisher (private communication).
[14] B. T. Ahlburn and A. K. Ramdas, Bull. Am. Phys. Soc. **14**, 396 (1969); Phys. Letters **29A**, 135 (1969).

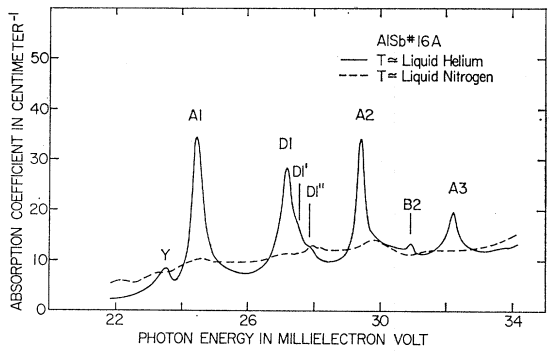

FIG. 1. Excitation spectrum of acceptors in an AlSb sample with room-temperature hole concentration $p(300°K) \approx 3 \times 10^{15}$ cm^{-3}.

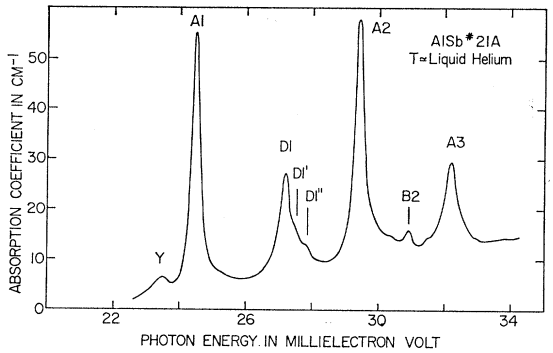

FIG. 2. Excitation spectrum of acceptors in an AlSb sample with $p(300°K) \approx 9 \times 10^{15}$ cm^{-3}. This sample was cut from the same ingot as was the sample of Fig. 1.

antimonide and their piezospectroscopic effects. The purpose of the present paper is to give a detailed account of this work.

II. EXPERIMENTAL PROCEDURE

Perkin-Elmer double-pass grating monochromators (Model No. 112G) were used for the measurements reported here. These monochromators were equipped with Bausch & Lomb plane-blazed reflection gratings. The experimental procedures and sample preparation techniques have been described elsewhere.[10] The samples used in these investigations were obtained from Bell & Howell.[15] The aluminum antimonide (AlSb) ingots were grown by the Czochralski technique without any intentional doping. At the present state of the art such material apparently always turns out to be p-type. The samples used have room-temperature hole concentrations in the range 3×10^{15}–5×10^{16} cm^{-3}.[15] The acceptor photoexcitation lines were observed to lie mostly to the long-wavelength side of the reststrahlen band at 31.4 μ.[16] For these lines the long-wavelength limit of the reflectivity, $R = 0.360$,[16] was used to calculate the absorption coefficient. For the lines occurring on the short-wavelength side of the reststrahlen band, the short-wavelength limit $R = 0.260$ was used.[16]

III. EXPERIMENTAL RESULTS AND DISCUSSION: ZERO-STRESS RESULTS

The absorption spectra measured at liquid-helium and liquid-nitrogen temperatures in a sample of p-type AlSb having a room-temperature hole concentration $p(300°K) \approx 3 \times 10^{15}$ cm^{-3} are presented in Fig. 1. In Fig. 2 is shown the helium-temperature absorption spectrum of a sample having $p(300°K) \approx 9 \times 10^{15}$ cm^{-3}. This sample was cut from the bottom of the same ingot from which the sample of Fig. 1 was cut. As can be seen in both figures, four strong, well-resolved lines, labelled $A1$, $D1$, $A2$, and $A3$, are observed at liquid-helium temperature. Two weak shoulders, denoted by $D1'$ and $D1''$ occur on the high-energy side of $D1$. In addition, two weak lines labelled Y and $B2$ are observed. Lines $A1$, $A2$, and $A3$, are much stronger in Fig. 2 than in Fig. 1, as would indeed be expected on the basis of the room-temperature hole concentrations of the respective samples.[15] On the other hand, lines Y and $D1$ do not show a corresponding increase in intensity. At liquid-nitrogen temperature, the absorption lines have all but vanished, although some structure is observable near the positions of Y, $A1$, $D1''$, and $A2$. In the range where the above spectra are observed, the samples are opaque at room temperature; free-hole absorption and inter-valence-band absorption[17] would be expected to contribute to this opacity. At the high-energy end of this region it is possible that the width of the reststrahlen band at 300°K also contributes to the absorption. None of the above lines has been observed in n-type AlSb.[10] From these observations we conclude that lines $A1$, $A2$, and $A3$ do indeed arise from photoexcitation of holes bound to the same type of acceptor center. On the other hand, no definite conclusions about the origin of lines $D1$, $B2$, and Y can be reached on the basis of the results presented so far.

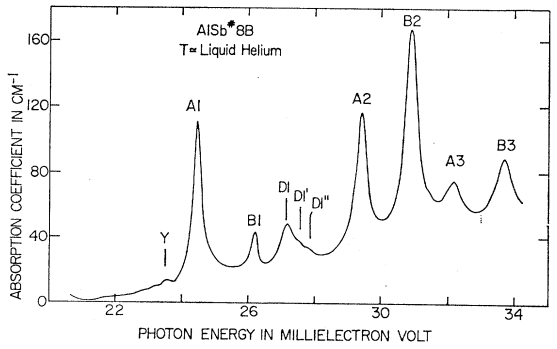

FIG. 3. Excitation spectrum of an AlSb sample having $p(300°K) \approx 5 \times 10^{16}$ cm^{-3}.

[15] Bell & Howell Research Laboratories, 360 Sierra Madre Villa, Pasadena, Calif. 91109. The carrier concentrations quoted in this publication are from the data supplied by the manufacturer.

[16] W. J. Turner and W. E. Reese, Phys. Rev. **127**, 126 (1962).

[17] R. E. Braunstein and E. O. Kane, J. Phys. Chem. Solids **23**, 1423 (1962).

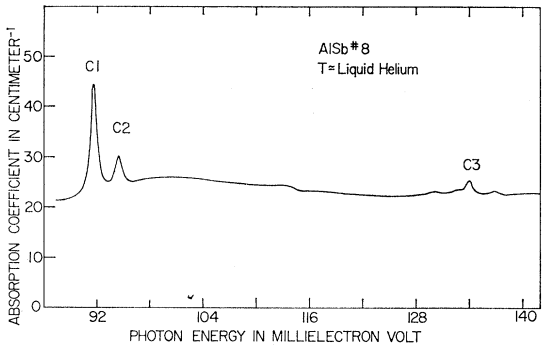

FIG. 4. Absorption spectrum of a p-type AlSb sample in the range 86–140 meV. $C1$ and $C2$ are acceptor photoexcitation lines, while $C3$ is the one-phonon replica of $C1$; $p(300°\text{K})\approx 5\times 10^{16}$ cm^{-3}.

The absorption spectrum observed at liquid-helium temperature in a p-type sample with $p(300°\text{K})\approx 3\times 10^{16}$ cm^{-3} is presented in Fig. 3. This sample was cut from a different ingot than that of Figs. 1 and 2. Lines $A1$, $A2$, and $A3$ have increased markedly in intensity. Line Y, on the other hand, is barely discernible on the low-energy wing of $A1$. In addition to the A lines and line $D1$, three well-resolved lines labelled $B1$, $B2$, and $B3$ are observed. Line $B2$, the strongest of the B lines, occurs at the position of the weak line labelled $B2$ in the preceding figures. Anticipating the results to be presented below, line Y does not show any significant effects when the sample is subjected to uniaxial compressions sufficiently large to produce sizable splittings of the A lines. This is characteristic of vibrational lines, for which very large stresses are required to produce observable effects.[18] For this reason, and because its intensity is not correlated with the intensities of either the A lines or the B lines, line Y appears to be of vibrational origin. Line $D1$, however, does show observable stress effects and hence must be of electronic origin. Since its intensity is correlated with neither the A lines nor the B lines, it may be associated with a third type of acceptor center.

TABLE I. Energies and spacings of lines observed in p-type aluminum antimonide.

Line No.	Energy (meV)	Spacing between lines	Spacing (meV)
$A1$	24.66±0.06	$A3$ & $A2$	2.78±0.12
$B1$	26.21±0.04	$B3$ & $B2$	2.78±0.19
$D1$	27.17±0.06	$C2$ & $C1$	2.78±0.32
$D1'$	27.53±0.10	$A2$ & $A1$	4.95±0.11
$D1''$	27.87±0.09	$B2$ & $B1$	4.68±0.13
$A2$	29.41±0.05		
$B2$	30.90±0.09		
$A3$	32.19±0.07		
$B3$	33.68±0.10		
$A4$[a]	65.0 ±0.5		
$A5$[a]	67.4 ±0.2		
$C1$	91.68±0.12		
$C2$	94.46±0.20		
$C3$[a]	134.0 ±0.2		

[a] Attributed to a hole photoexcitation transition accompanied by the simultaneous emission of a phonon.

As shown in Fig. 4, yet another acceptor photoexcitation spectrum is observed for the same sample as that in Fig. 3. At liquid-helium temperature, two sharp lines labelled $C1$ and $C2$ are observed. These lines are not observed at liquid-nitrogen or at room temperatures. The high background absorption in this spectral region at liquid-helium temperature may arise from photo-ionization of the shallower acceptors. Line $C3$, at 134.0 meV, is energetically equivalent to the hole photoexcitation transition which gives rise to $C1$ accompanied by the simultaneous creation of an LO_Γ phonon. A search was made to locate counterparts of $C3$ for the A and B lines. Two very weak lines labelled $A4$ and $A5$ are observed at 65 and 67.4 meV corresponding to the transition giving rise to $A1$ accompanied by the creation of a TO_Γ and an LO_Γ phonon, respectively. In all three cases, the hole excitation plus phonon emission transitions are weaker than the donor photoexcitation plus phonon emission transitions observed in n-type AlSb.[10]

The energies of the lines attributed to acceptors in AlSb are presented in Table I. It should be noted that the A, B, and D lines, with the exception of $B3$, lie at energies consistent with the 33-meV value reported by Stirn and Becker[19] for the ionization energy of an unidentified acceptor in AlSb from the same ingot as the sample of Fig. 3. Although line $B3$, at 33.68 meV, lies above this value, the experimental uncertainty in determining the ionization energy from electrical measurements is presumably large enough for this line to lie below it. The observation of the C lines in samples having $p(300°\text{K})\approx 5\times 10^{16}$ cm^{-3} and its absence in samples cut from the ingot with lower hole concentration are consistent with Hall-effect data from Bell & Howell for these samples which indicate the existence in the former ingot of an acceptor which is deeper than those in the latter ingot.[20]

From Table I it is readily seen that the spacings between lines $A3$ and $A2$, $B3$ and $B2$, and $C2$ and $C1$ are all equal to 2.78 meV. Inspection of the three sets of spectra indicates, moreover, that the intensity ratios $I(A2)/I(A3)$, $I(B2)/I(B3)$, and $I(C1)/I(C2)$ are very similar. Furthermore, the spacing between lines $A2$ and $A1$, 4.95±0.11 meV, is close to the spacing between lines $B2$ and $B1$, 4.68±0.13 meV. This behavior is characteristic of bound hole states described by the effective-mass theory, and suggests that such an approach may have some merit for describing acceptor states in AlSb. Theoretical calculations for acceptor states in AlSb have yet to be performed. It is, however, useful to characterize the symmetries of the states involved in the transitions. This can be achieved from piezospectroscopic studies.

[18] G. S. Hobson and E. G. S. Paige, Proc. Phys. Soc. (London) 88, 437 (1966).

[19] R. J. Stirn and W. M. Becker, Phys. Rev. 148, 907 (1966).

[20] R. K. Willardson (private communication).

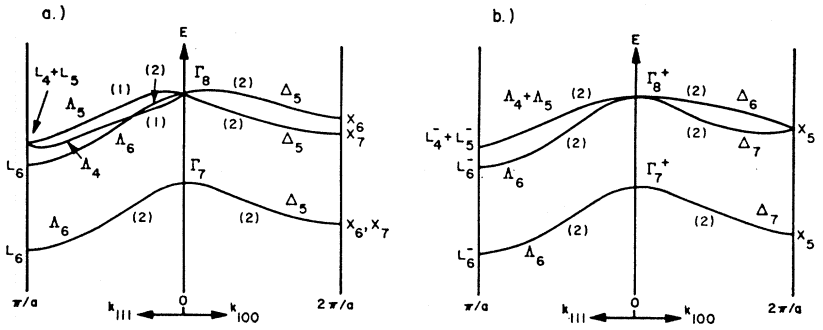

FIG. 5. Theoretical valence-band structure (not to scale) of (a) a III-V semiconductor, and (b) of a homopolar group-IV semiconductor. Spin-orbit effects are included. The numbers in parentheses denote the degeneracies of the various valence-band branches. The group theoretical notation is that of Ref. 21. (Reproduced from Ref. 1.)

IV. PIEZOSPECTROSCOPIC EFFECTS

A. Theoretical Considerations

In order to characterize the symmetry of the acceptor states in the effective-mass approach, it is necessary to consider the symmetry of the valence band with which they are intimately associated. The valence band of the III-V compounds is shown in Fig. 5(a); this has been deduced theoretically by Dresselhaus,[21] Parmenter,[22] and Kane.[23] In this model, the valence-band maxima are shifted slightly away from $\mathbf{k}=0$, with the highest maxima lying along the $\langle 111\rangle$ directions. Eight maxima are expected along the $\langle 111\rangle$ directions, while six and 12 maxima are expected along the $\langle 100\rangle$ and $\langle 110\rangle$ directions, respectively. In addition, the twofold degenerate upper Λ_6 level is expected to have its maximum at $\mathbf{k}=0$. Also, the lower Λ_6 band, which is depressed by the spin-orbit interaction, is twofold degenerate and has its maximum at $\mathbf{k}=0$. The shift of the valence-band maxima away from $\mathbf{k}=0$ is a consequence of the absence of the center of inversion in the zinc-blende lattice of the III-V compounds; i.e., the shift arises because of the dissimilarities between the group-III and group-V atoms comprising the lattice. Considering the dissimilarities between the aluminum and antimony atoms, this effect may be larger for AlSb than for some of the other III-V compounds such as, for example, InSb. If in contrast to this, the masses and electronic charge distributions of the group-III and group-V atoms tend to become nearly equal, the maxima should lie closer to $\mathbf{k}=0$, and the valence-band structure should then tend to resemble that of a homopolar semiconductor like germanium, which has the valence-band structure shown in Fig. 5(b). It should be noted that the magnitudes of the shifts of the valence-band maxima away from $\mathbf{k}=0$ also depend on the spin-orbit splitting,[23] which is ~ 0.75 eV in AlSb.[17]

It is apparent that predictions about the symmetries of acceptor states closely linked to the valence-band structure depicted in Fig. 5(a), including their behavior under stress, would be, in principle, complicated. From the experimental results to be presented in Sec. IV B, however, it will be clear that the stress-induced behavior of the acceptor lines can be described with success by assuming the simpler germaniumlike valence band for AlSb and T_d site symmetry for the acceptor; the acceptor states will then have the same symmetry as those of group-III acceptors in silicon or germanium.

Good summaries of the theory of the acceptor states associated with group-III atoms in silicon or germanium have been given by Onton *et al.*[6] and by Fisher and Ramdas.[24] The acceptor ground-state wave functions form a basis for the irreducible representation Γ_8 of the double group $\bar{T}_d$,[25] while the excited-state wave functions form a basis for either Γ_6, Γ_7, or Γ_8. The upper valence band, which can be characterized by an angular momentum quantum number $J=\frac{3}{2}$ and is fourfold degenerate at $\mathbf{k}=0$, splits into two twofold-degenerate bands when a uniaxial stress is applied. For an applied uniaxial force $\mathbf{F}$, the $M_J=\pm\frac{3}{2}$ states separate from the $M_J=\pm\frac{1}{2}$ states according to

$$\begin{aligned}&\Delta E_{\pm 3/2}=+\tfrac{1}{2}\Delta_{100},\\ &\Delta E_{\pm 1/2}=-\tfrac{1}{2}\Delta_{100}\quad \text{for}\quad \mathbf{F}\|\langle 100\rangle,\end{aligned}\tag{1}$$

where $\Delta_{100}=2b(s_{11}-s_{12})T$, and according to

$$\begin{aligned}&\Delta E_{\pm 3/2}=+\tfrac{1}{2}\Delta_{111},\\ &\Delta E_{\pm 1/2}=-\tfrac{1}{2}\Delta_{111}\quad \text{for}\quad \mathbf{F}\|\langle 111\rangle,\end{aligned}\tag{2}$$

where $\Delta_{111}=(d/\sqrt{3})s_{44}T$, both Δ_{100} and Δ_{111} being measured in terms of hole energy. Here b and d are the deformation potential constants of the valence band for uniaxial stress along the $\langle 100\rangle$ and $\langle 111\rangle$ directions, respectively[26]; s_{11}, s_{12}, and s_{44} are the elastic compliance constants; T is the stress produced by $\mathbf{F}$ and is defined to be positive for tensile force. Since the splittings given by Eqs. (1) and (2) have been deduced from the symmetry of the valence band, identical relationships should hold for the splittings of the Γ_8 acceptor states, although, in principle, the deformation potential constants can be different for each state. An excited state

[21] G. Dresselhaus, Phys. Rev. **100**, 580 (1955).
[22] R. H. Parmenter, Phys. Rev. **100**, 573 (1955).
[23] E. O. Kane, J. Phys. Chem. Solids **1**, 249 (1957).
[24] P. Fisher and A. K. Ramdas, in *Physics of the Solid State*, edited by S. Balakrishna, M. Krishnamurthy, and B. Ramachandra Rao (Academic Press Inc., London, 1969).
[25] For the notation used here, see G. F. Koster, J. O. Dimmock, R. G. Wheeler, and H. Statz, *Properties of the Thirty-Two Point Groups* (MIT Press, Cambridge, Mass., 1967).
[26] G. L. Bir, E. I. Butikov, and G. E. Picus, J. Phys. Chem. Solids **24**, 1467 (1963).

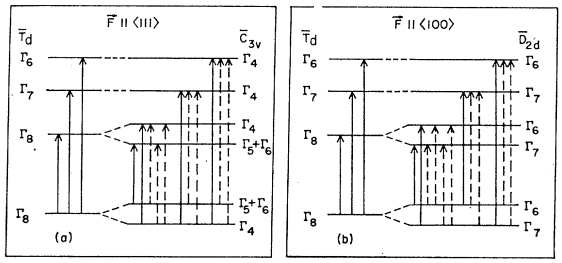

FIG. 6. Behavior of transitions from a Γ_8 ground state to Γ_6, Γ_7, and Γ_8 excited states of the double group T_d for (a) $\mathbf{F}\|\langle 111\rangle$, and for (b) $\mathbf{F}\|\langle 100\rangle$. The solid arrows are for $\mathbf{E}\|\mathbf{F}$, while the dashed arrows are for $\mathbf{E}\perp\mathbf{F}$. The group-theoretical notation is that of Ref. 25.

having wave functions which form a basis for either Γ_6 or Γ_7 will not split, however, because the twofold Kramers degeneracy must be retained under stress.[27,28] Using group-theoretical arguments, the symmetries of the stress-induced sublevels of a given state and the selection rules for optical transitions may be deduced in the usual manner. Splittings of the various types of states and the selection rules are shown in Fig. 6 for $\mathbf{F}\|\langle 111\rangle$ and $\mathbf{F}\|\langle 100\rangle$.

Group-theoretical considerations may also be used to calculate the relative intensities of the various stress-induced components of a given line if the symmetries of the initial and final states of the components are known. Following the theoretical treatment of Kaplyanskii,[29] Onton *et al.*[6] have calculated the intensities of the various stress-induced components of group-III acceptor lines in silicon and germanium. The ratio of two undetermined parameters, C_ψ and C_φ, appears in the calculation of relative intensities for the stress-induced components of a line which arises from a $\Gamma_8 \rightarrow \Gamma_8$ transition in the absence of stress. Only one undetermined parameter occurs in the calculation of the intensities for $\Gamma_8 \rightarrow \Gamma_6$ or $\Gamma_8 \rightarrow \Gamma_7$ transitions; thus the relative intensities of stress-induced components of such lines may be calculated exactly. The relative intensities of the stress-induced components of a $\Gamma_8 \rightarrow \Gamma_8$ line are shown in Fig. 7 as a function of the ratio C_ψ/C_φ for $\mathbf{F}\|\langle 111\rangle$ and $\mathbf{F}\|\langle 100\rangle$.

B. Experimental Results and Discussion

The effects of a compressive force $\mathbf{F}$ along $\langle 111\rangle$ on $D1$, $B2$, and the A lines are shown in Figs. 8 and 9; from the experimental conditions, it was estimated that the stress applied to the sample was substantially larger for the spectrum in Fig. 9 than for that in Fig. 8. In Figs. 10 and 11, the behavior of these lines for $\mathbf{F}\|\langle 100\rangle$ is shown; here the magnitude of the applied stress is larger for the spectrum in Fig. 11 than for that in Fig. 10.

The data for $\mathbf{F}\|\langle 100\rangle$ are summarized in Fig. 12, where the positions of the stress-induced components are plotted versus $\Delta_{100}{}^g$, which is the separation between $A1.4(\perp)$ and $A1.2(\perp)$. It will be seen that $\Delta_{100}{}^g$ has been attributed to the ground-state splitting for the A lines. Despite the measures taken, some of the stronger water vapor lines in this spectral region frequently appeared with sufficient strength to interfere with the identification of some of the weaker stress-induced components. The most persistent water vapor lines occur at 25.11 meV (49.4 μ), 25.84 meV (47.9 μ), 28.2 meV (44 μ), 31.48 meV (39.4 μ), and 33.00 meV (37.6 μ); this has been taken into account in Fig. 12.

For $\mathbf{F}\|\langle 111\rangle$, as can be seen from Fig. 8, two components are observed for line $A2$ when the electric vector of the radiation, $\mathbf{E}$, is along $\mathbf{F}$. Here one component

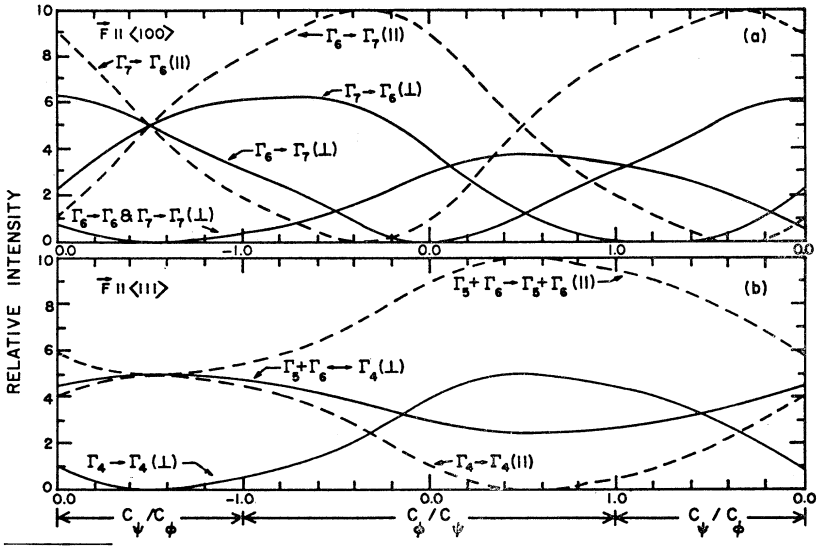

FIG. 7. Relative intensities of transitions between the stress-induced sublevels of two Γ_8 states for (a) $\mathbf{F}\|\langle 100\rangle$ and (b) $\mathbf{F}\|\langle 111\rangle$ as a function of the parameter C_φ/C_ψ. Note that the range $|C_\varphi/C_\psi| \geq 1$ has been plotted as C_ψ/C_φ. Solid lines and dashed lines here represent transitions for $\mathbf{E}\perp\mathbf{F}$ and $\mathbf{E}\|\mathbf{F}$, respectively. (Reproduced from Ref. 6 with the additional labels of Ref. 30.)

[27] W. Kohn, in *Solid State Physics*, edited by F. Seitz and D. Turnbull (Academic Press Inc., New York, 1957), Vol. 5, p. 257.
[28] V. Heine, *Group Theory in Quantum Mechanics* (Pergamon Press, Inc. New York, 1960), p. 164.
[29] A. A. Kaplyanskii, Opt. Spektrosk. **16**, 1031 (1964) [English transl.: Opt. Spectry. **16**, 557 (1964)].

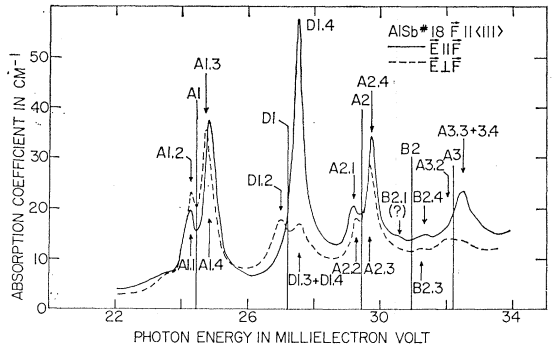

FIG. 8. Excitation spectrum of an AlSb sample with $p(300°K) \approx 3\times10^{15}$ cm^{-3} for $\mathbf{F}\|\langle111\rangle$. Liquid helium used as coolant. Zero-stress positions are denoted by solid vertical lines.

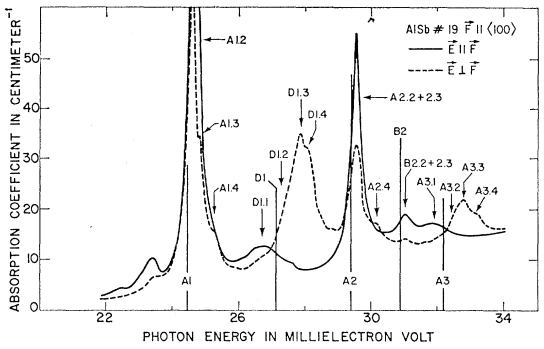

FIG. 10. Excitation spectrum of an AlSb sample with $p(300°K) \approx 3\times10^{15}$ cm^{-3} for $\mathbf{F}\|\langle100\rangle$. Liquid helium used as coolant. Zero-stress positions are denoted by solid vertical lines.

occurs on either side of the zero-stress position. Two components, one on either side of the zero-stress position, are also observed for $\mathbf{E}\perp\mathbf{F}$. In Fig. 8 the perpendicular components appear to lie just inside the parallel components; however, the separation between the respective perpendicular and parallel components is within the experimental accuracy of the line positions. As can be seen from a comparison of Figs. 8 and 9, both low-energy components are absent in the latter; other measurements, not reproduced here, show that they decrease in intensity with increasing stress. In addition, the high-energy components split slightly further from the zero-stress positions than do the low-energy components. As can also be seen in Fig. 9, the parallel components of $A2$ as well as those of the other lines appear to gain intensity relative to the perpendicular components as the stress is increased. To the extent that it can be determined, the behavior of the very weak line $B2$ is similar to that of line $A2$ for this direction of applied force. In order that two components be observed for $\mathbf{E}\|\mathbf{F}$ with $\mathbf{F}\|\langle111\rangle$, lines $A2$ and $B2$ can be attributed to $\Gamma_8\rightarrow\Gamma_8$ transitions. Furthermore, the decrease in intensity of the low-energy components with increasing stress provides clear evidence that the ground state is a Γ_8 state. The application of stress lifts the degeneracy, and depopulation of the upper ground-state sublevel with increasing stress leads to the decrease in intensity for the lower-energy components which originate from this state. The behavior of lines $A2$ and $B2$ can be interpreted in terms of Fig. 13(a). The high-energy component $A2.4$ has not been observed for $\mathbf{E}\perp\mathbf{F}$. From Fig. 7 it can be seen that the intensity of this component, which arises from the $\Gamma_4\rightarrow\Gamma_4$ transition, is vanishingly small for $-1.0<C_\psi/C_\varphi<0$. This interpretation is similar to that given for line 2 of the group-III acceptors in silicon.[6] However, the separation between the perpendicular and parallel components is significantly larger for silicon than for AlSb. This indicates that the ratio of the excited-state splitting to the ground-state splitting, $\Delta_{111}'/\Delta_{111}^0$, is smaller for these lines than was observed for silicon. As Δ_{111}' approaches zero, of course, the respective high- and low-energy perpendicular and parallel components become coincident. This is the interpretation given for the D lines of group-III acceptors in germanium.[9,30]

The ordering of the stress-induced sublevels of the ground state of line $A2$ was chosen to be the same as for acceptors in silicon[6] and germanium.[9,30] For acceptors in silicon, the observation of the very weak

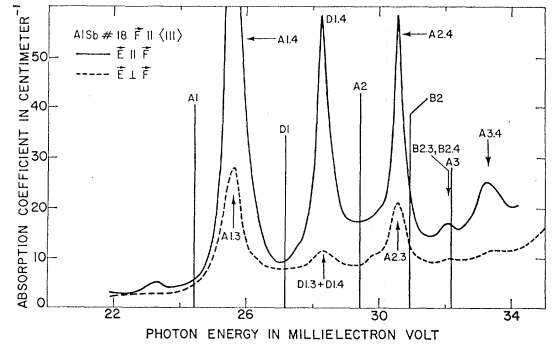

FIG. 9. Excitation spectrum of an AlSb sample with $p(300°K) \approx 3\times10^{15}$ cm^{-3} for $\mathbf{F}\|\langle111\rangle$. The stress here is larger than that for Fig. 8. Liquid helium used as coolant.

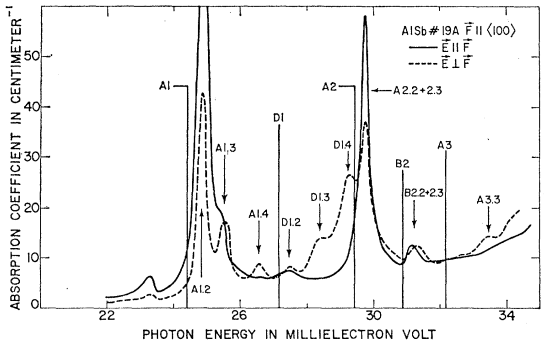

FIG. 11. Excitation spectrum of an AlSb sample with $p(300°K) \approx 3\times10^{15}$ cm^{-3} for $\mathbf{F}\|\langle100\rangle$. The stress here is greater than that of Fig. 10. Liquid helium used as coolant.

[30] R. L. Jones, Ph.D. thesis, Purdue University, 1968 (unpublished).

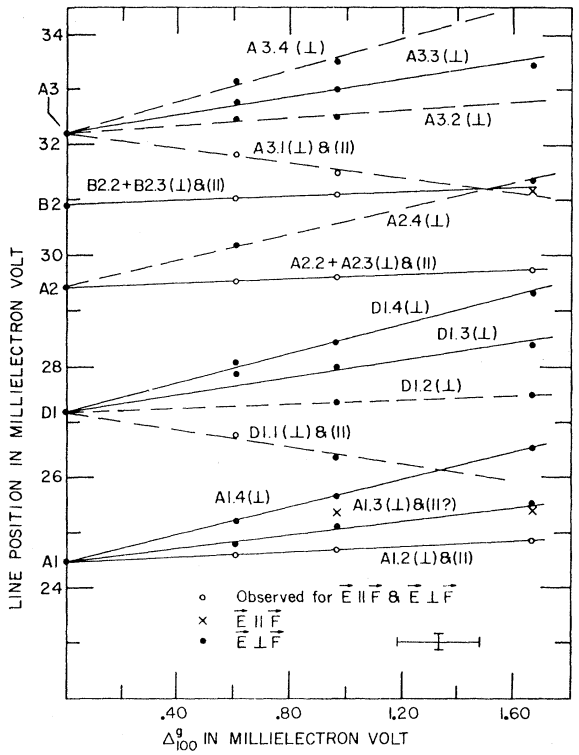

FIG. 12. Positions of stress-induced components as a function of ground state splitting $\Delta_{100}{}^{g}$ for $\mathbf{F}\|\langle 100\rangle$. The dashed lines denote components whose existence has not been definitely established.

high-energy component corresponding to $A2.4(\perp)$, as well as the behavior of the $2p'$ line established that the Γ_4 sublevel of the ground state was the lower. Since $A2.4$ has not been observed for $\mathbf{E}\perp\mathbf{F}$, for AlSb an equally consistent interpretation may be advanced if the $\Gamma_5+\Gamma_6$ sublevel is the lower ground-state level while the Γ_4 sublevel of the excited state lies below the $\Gamma_5+\Gamma_6$ excited-state level. In either case, the ground-state splitting is measured by the separation between $A2.4$ ($\|$) and $A2.2$ ($\perp$), where the labels for the transitions are retained for both orderings. The fact that the high-energy components shift somewhat further from the zero-stress position than do the low-energy components suggests a slight shift of the centers of gravity of the ground and excited states relative to each other.

As can be seen in Fig. 10, line $A2$ shows one strong component, labelled $A2.2+A2.3$, for $\mathbf{F}\|\langle 100\rangle$. This component is observed for both polarizations and occurs close to the zero-stress position, although it does shift slightly towards higher energies with increasing stress. There is also some evidence of a higher-energy component $A2.4$ for $\mathbf{E}\perp\mathbf{F}$, as may be seen in Figs. 10 and 12. To the extent that it can be determined, the behavior of line $B2$ for $\mathbf{F}\|\langle 100\rangle$ is again similar to that of $A2$. The stress-induced behavior of line $A2$ can be interpreted on the basis of Fig. 13(b). A single component labelled $A2.2+A2.3$, which is a superposition of the $\Gamma_7\rightarrow\Gamma_6$ and $\Gamma_6\rightarrow\Gamma_7$ transitions, is observed for both $\mathbf{E}\perp\mathbf{F}$ and $\mathbf{E}\|\mathbf{F}$ when the excited-state splitting $\Delta_{100}{}'$ equals the ground-state splitting $\Delta_{100}{}^{g}$. The slight shift of these components above the zero-stress position as the stress is increased probably signifies that the centers of gravity of the ground and excited states shift slightly relative to one another. Component $A2.1$ ($\perp$) is not observed, and the high-energy component $A2.4$ ($\perp$) is at best very weak. As can be seen in Fig. 7(a), these components should be weak for $-1.0<C_\psi/C_\varphi<0.0$, which is consistent with the range for this ratio deduced from the behavior for $\mathbf{F}\|\langle 111\rangle$. Furthermore, the low-energy component would be weakened further relative to the high-energy component due to depopulation effects, so that it could not be observed as readily as the high-energy component. The stress-induced behavior of line $A2$ for $\mathbf{F}\|\langle 100\rangle$ can also be interpreted consistently if the ordering of both the ground- and excited-state sublevels is inverted with respect to that in Fig. 13(b).

The behavior of line $A1$ for $\mathbf{F}\|\langle 111\rangle$ is very similar to that of $A2$, as is clear from Fig. 8; hence it can be interpreted in the same manner. It is apparent from Figs. 10–12, on the other hand, that its behavior for $\mathbf{F}\|\langle 100\rangle$ is more complicated than that of $A2$; three components, denoted by $A1.2$, $A1.3$, and $A1.4$, are clearly observed for $\mathbf{E}\perp\mathbf{F}$. Although the presence of persistent water vapor lines at 25.11 and 25.84 meV interferes to some extent in determining the positions of $A1.3$ ($\perp$) and $A1.4$ ($\perp$), the fact that their positions extrapolate back to the zero-stress position of $A1$ in Fig. 12 for $\Delta_{100}{}^{g}=0$ strengthens the interpretation that they are indeed stress-induced components of $A1$. For $\mathbf{E}\|\mathbf{F}$ two components are observed. The strength of the component $A1.2$ ($\|$) is such that the transmission goes to zero at its peak position and hence, in Figs. 10 and 11, the absorption maxima are not shown. The position

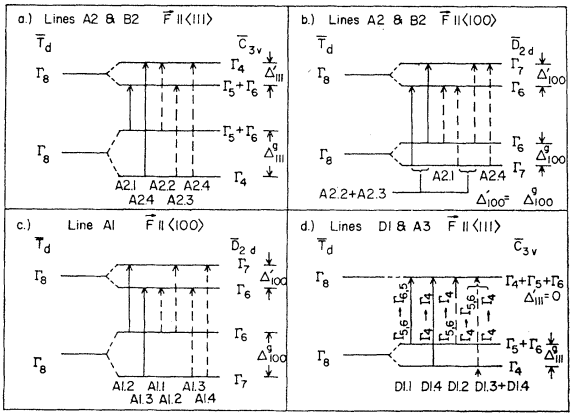

FIG. 13. Energy-level splittings postulated for describing the stress-induced behavior of various acceptor photoexcitation lines. Transitions for $\mathbf{E}\|\mathbf{F}$ are denoted by solid arrows, while those for $\mathbf{E}\perp\mathbf{F}$ are denoted by dashed arrows.

of the weaker component $A1.3$ ($\|$) is difficult to determine accurately, but it appears to be coincident with that of $A1.3$ ($\perp$). The only component which appears to decrease in intensity as the stress increases is $A1.2$ ($\perp$); it has not been possible to establish that a corresponding decrease in intensity occurs for $A1.2$ ($\|$) in view of its high intensity. In addition to these features, $A1.2$ shifts to the high-energy side of its zero-stress position by approximately the same amount as $A2.2$ $+A2.3$ shifts from its zero-stress position; this similarity in the stress-induced behavior of the two lines suggests that a similar energy-level scheme might be used to describe both $A1$ and $A2$. However, as can be seen in Figs. 10 and 11, the observation of $A1.3$ ($\perp$), $A1.4$ ($\perp$), and $A1.3$ ($\|$), along with the depopulation effect observed for $A1.2$ ($\perp$) indicates that this is not the case. Most of the observed features may be accounted for on the basis of Fig. 13(c), where the excited-state splitting $\Delta_{100}'<\Delta_{100}^{g}$. Here the ground-state splitting Δ_{100}^{g} corresponds to the separation between $A1.4$ ($\perp$) and $A1.2$ ($\perp$). Once again, a center-of-gravity shift is required for the $A1.2$ components to shift to the high-energy side of the zero-stress position of $A1$. The failure to observe $A1.1$ ($\perp$) and the low intensity of $A1.4$ ($\perp$) suggests $-1.0<C_{\psi}/C_{\varphi}<0.0$ for $A1$; this is consistent with the range of C_{ψ}/C_{φ} values deduced from its behavior for $\mathbf{F}\|\langle 111\rangle$. As before, the low-energy component $A1.1$ ($\perp$) would be weakened relative to $A1.4$ ($\perp$) by depopulation effects. In addition, for $\mathbf{F}\|\langle 100\rangle$ the decrease in intensity of line $A1.2$ ($\perp$) with increasing stress, is expected on the basis of Fig. 13(c), because it originates from the upper ground state. From Figs. 10 and 11, it is obvious that the intensity of $A1.2$ ($\|$) is substantially greater than that of $A1.2$ ($\perp$), which is in turn significantly larger than the intensity of any of the other stress-induced components. Examination of Fig. 7(a) indicates that this is not expected for any value of C_{ψ}/C_{φ}. This feature is thus inconsistent with the line of reasoning adopted to explain the above piezospectroscopic effects.

When the sample is subjected to a $\langle 111\rangle$ compression, line $D1$ splits into two components for $\mathbf{E}\perp\mathbf{F}$, one on each side of the zero-stress position (see Figs. 8 and 9). The component observed for $\mathbf{E}\|\mathbf{F}$ is coincident with the high-energy component for $\mathbf{E}\perp\mathbf{F}$. The low-energy component for $\mathbf{E}\perp\mathbf{F}$ is absent from the spectrum observed with larger stress in Fig. 9. As far as can be determined, the weak line $A3$ exhibits similar behavior. Considering their behavior for $\mathbf{F}\|\langle 111\rangle$ only, $D1$ and $A3$ could be attributed to $\Gamma_8\rightarrow\Gamma_6$ or Γ_7 transitions, as shown in Fig. 6(a). However, this interpretation is inconsistent with the results shown in Figs. 10–12 for $\mathbf{F}\|\langle 100\rangle$, since four stress-induced components are observed. It is possible to interpret the behavior of $D1$ and $A3$ for $\mathbf{F}\|\langle 111\rangle$ in terms of Fig. 13 (d), with the excited-state splitting $\Delta_{111}'=0$ and with the ordering of the ground states reversed. Examination of Fig. 7(b) indicates

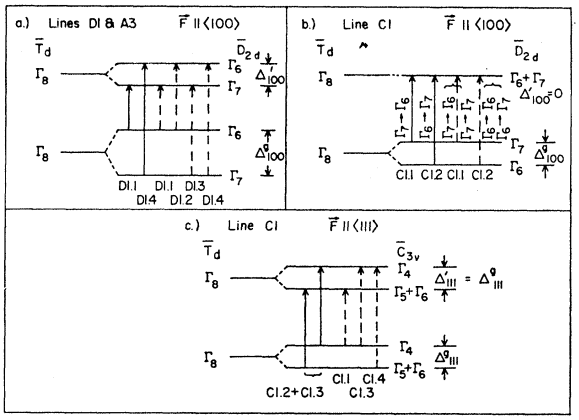

FIG. 14. Energy-level splittings postulated for describing the stress-induced behavior of various acceptor photoexcitation lines. Transitions for $\mathbf{E}\|\mathbf{F}$ are denoted by solid arrows, while those for $\mathbf{E}\perp\mathbf{F}$ are denoted by dashed arrows.

not only that the low-energy parallel component $D1.1$ ($\|$), which is attributed to the $\Gamma_5+\Gamma_6\rightarrow\Gamma_5+\Gamma_6$ ($\|$) transition in Fig. 13 (d), can not vanish, but also that it must be of greater intensity than $D1.4$ ($\|$). This is obviously inconsistent with the observed features. If, however, the Γ_4 ground-state sublevel lies *above* the $\Gamma_5+\Gamma_6$ ground-state level, the low-energy parallel component would then arise from the $\Gamma_4\rightarrow\Gamma_4$ ($\|$) transition, which has very low intensity for C_{φ}/C_{ψ} in the range 0–1.0. Moreover, the high-energy parallel component should then be the most intense, which is indeed the case. Should this interpretation of the stress-induced behavior of lines $D1$ and $A3$ for $\mathbf{F}\|\langle 111\rangle$ be correct, the ground-state ordering for lines $A1$ and $A2$ must also have the Γ_4 level lying above the $\Gamma_5+\Gamma_6$ level. It has already been noted that the behavior of these lines may be interpreted with equal consistency, provided that the ordering of the excited-state levels has the Γ_4 level *below* the $\Gamma_5+\Gamma_6$ level. This would imply that the ground-state deformation potential d' [26] for AlSb is of opposite sign to that observed in silicon[6] and germanium.[9,30]

From Figs. 10–12, it is seen that for $\mathbf{F}\|\langle 100\rangle$, $D1$ splits into two very weak perpendicular components, labelled $D1.1$ ($\perp$) and $D1.2$ ($\perp$), and two fairly strong perpendicular components, labelled $D1.3$ ($\perp$) and $D1.4$ ($\perp$). Only the low-energy parallel component $D1.1$ ($\|$) is observed, and it can be seen only for the measurement of Fig. 10, where the stress is smaller than for Fig. 11. As far as can be determined, the behavior of line $A3$ is again similar to that of $D1$. This behavior may be interpreted on the basis of Fig. 14(a), where the Γ_7 level is the lower stress-induced sublevel for both the ground and excited states, and $\Delta_{100}'<\Delta_{100}^{g}$. The occurrence of three components on the high-energy side of the zero-stress position may again be attributed to a shift of the center of gravity of the ground and excited states relative to each other. The

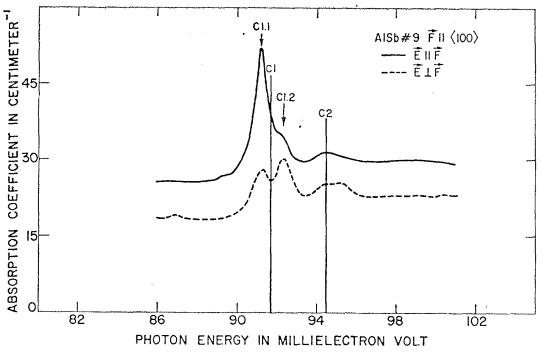

FIG. 15. Behavior of the C lines for $\mathbf{F}\|\langle 100\rangle$; $p(300°\mathrm{K}) \approx 5\times 10^{16}$ cm^{-3}. Liquid helium used as coolant. Zero-stress positions are denoted by solid vertical lines.

ordering of the ground- and excited-state sublevels must be the same if the lowest-energy component is to appear for $\mathbf{E}\|\mathbf{F}$. The high-energy parallel component $D1.4$ ($\|$), which is attributed to the $\Gamma_7 \rightarrow \Gamma_6$ ($\|$) transition, has not been observed, which suggests a value for C_φ/C_ψ in the range -0.8–0. In order to maintain consistency with the range of C_φ/C_ψ deduced for these lines with $\mathbf{F}\|\langle 111\rangle$, it must be taken ~ 0. Including depopulation effects, for $T \sim 15°\mathrm{K}$, the intensities of the various stress-induced components should be in the ratios $D1.4$ ($\perp$): $D1.3$ ($\perp$): $D1.2$ ($\perp$): $D1.1$ ($\perp$): $D1.4$ ($\|$): $D1.1$ ($\|$)::4:3:1.8:0:1:4.8 for the ground-state splitting in Fig. 10. The intensities of the perpendicular components agree at least qualitatively with this estimate, although nothing can be concluded about the intensity of $D1.2$ ($\perp$), which has not been resolved in this figure. The predicted intensities of the parallel components, however, are somewhat high. The ordering of levels in Fig. 14(a), if also valid for $A3$, would indicate that the deformation potential constant b' [26] for the ground state of an acceptor in AlSb is of the same sign as observed in silicon[6] and germanium.[7,9,30] Although the ordering in which the Γ_6 sublevels lie below the Γ_7 sublevels leads to the same polarization patterns as does the ordering in Fig. 14(a), this latter ordering is preferable on the grounds of intensity predictions.

It should be noted that this interpretation for $D1$ and $A3$ is different from that advanced by Dickey and Dimmock[9] and by Fisher and Jones[7,30] for the C lines of group-III acceptors in germanium, which show a behavior rather similar to these lines for $\mathbf{F}\|\langle 111\rangle$ and $\mathbf{F}\|\langle 100\rangle$. The C line might be attributed[9,30] to a transition from the Γ_8 ground state to an excited state composed of a Γ_8 state degenerate with a Γ_7 state. This assignment was consistent with the theoretical calculation of hole binding energies by Mendelson and James.[31] No corresponding calculations exist for AlSb. If such an assignment were made for $D1$ and/or $A3$ in AlSb, the Γ_4 ground-state level could again be the lower sublevel for $\mathbf{F}\|\langle 111\rangle$, and d' for AlSb would be of the same sign as for germanium.

Due to the unavailability of suitable samples, the only information obtained about the stress behavior of the B lines was that gained for the very weak $B2$ line observed along with the A lines in the samples of lower hole concentration. In the samples in which $B2$ was readily observable, the high impurity concentrations necessitated using sample thicknesses which were too small for stress measurements to be performed.

The effects of $\mathbf{F}\|\langle 100\rangle$ and $\mathbf{F}\|\langle 111\rangle$ on the C lines are shown in Figs. 15–17. The experimental conditions were such that the stress was larger for the spectra in Fig. 17 than in Fig. 16.

For $\mathbf{F}\|\langle 100\rangle$, $C1$ splits into two components, one on either side of the zero-stress position. Each component appears for both $\mathbf{E}\perp\mathbf{F}$ and $\mathbf{E}\|\mathbf{F}$. The splitting is not completely symmetric in that the high-energy component shifts somewhat further away from the zero-stress position than does the low-energy component. None of the A lines, $B2$, or $D1$ displays a similar polarization pattern. If, however, the acceptor giving rise to $C1$ and $C2$ is again assumed to be at a site having T_d symmetry, the behavior can be interpreted on the basis of Fig. 14(b). In order for two components to be observed in each polarization, the simplest interpretation is to attribute $C1$ to a $\Gamma_8 \rightarrow \Gamma_8$ transition. For this energy-level scheme, the ground-state splitting $\Delta_{100}{}^g$ corresponds to the separation between $C1.1$ and $C1.2$. An equally consistent interpretation of the behavior of line $C1$ for $\mathbf{F}\|\langle 100\rangle$ is possible for the Γ_7 ground-state sublevel lying below the Γ_6 sublevel. Moreover, since the occurrence of depopulation effects has not been observed, the possibility that the excited state splits and that the ground state does not cannot be discounted. The splittings observed are not of sufficient magnitude to ascertain whether or not depopulation effects are present.

As can be seen in Figs. 16 and 17, line $C1$ broadens for $\mathbf{F}\|\langle 111\rangle$ but does not split into resolvable components. The line does decrease noticeably in intensity for $\mathbf{E}\perp\mathbf{F}$, however. It might be argued that the occurrence of the lines close to their zero-stress positions arises from equal splittings of the ground and excited states. The energy-level scheme which is most nearly consistent with the observed behavior of $C1$ is shown in Fig. 14(c), where the excited-state splitting $\Delta_{111}{}'$ has been taken equal to the ground-state splitting $\Delta_{111}{}^g$. The zero-stress component for $\mathbf{E}\|\mathbf{F}$ would then arise from a superposition of the $\Gamma_5+\Gamma_6 \rightarrow \Gamma_5+\Gamma_6$ ($\|$) and the $\Gamma_4 \rightarrow \Gamma_4$ ($\|$) transitions, and should not *decrease* in intensity with increasing stress as a result of depopulation effects. The zero-stress component for $\mathbf{E}\perp\mathbf{F}$ would arise from the $\Gamma_4 \rightarrow \Gamma_4$ ($\perp$) transition and should show depopulation effects, as observed. In addition to the zero-stress component, a low-energy and a

[31] K. S. Mendelson and H. M. James, J. Phys. Chem. Solids **25**, 729 (1964).

high-energy component, labelled $C1.1$ and $C1.4$, respectively, would be expected for $\mathbf{E}\perp\mathbf{F}$. These components would have their minimum intensity at $C_\varphi/C_\psi \approx 0.5$; neglecting depopulation effects they would be expected to have $\approx\frac{1}{5}$ the intensity of the parallel component, and approximately $\frac{1}{2}$ the intensity of $C1.3$ ($\perp$). As can be seen from Figs. 16 and 17, there is some qualitative support for this interpretation of $C1$. This interpretation implies that the deformation potential constant d' for the ground state of this acceptor is of opposite sign from those for the ground states of the group-III acceptors in silicon and germanium.

It has not been possible to observe any clearly resolved components of the very weak line $C2$ for either $\mathbf{F}\|\langle 100\rangle$ or $\mathbf{F}\|\langle 111\rangle$. Hence no interpretation is advanced for this line.

As yet, none of the acceptor photoexcitation lines has been studied for $\mathbf{F}\|\langle 110\rangle$.

V. CONCLUDING DISCUSSION

The experimental results of this paper have established the existence of four types of acceptor centers, A, B, C, and D in the AlSb crystals examined in the present investigations. The equality of the spacings between $A2$ and $A3$, $B2$ and $B3$, and $C1$ and $C2$ suggests that these lines arise from transitions to excited states which may be described in terms of an effective-mass-like approach; the final states for $A2$, $B2$, and $C1$ would thus be expected to have similar symmetry properties, as would the final states for $A3$, $B3$, and $C2$. The similarities in behavior of $A2$ and $B2$ under the application of uniaxial stress supports this assumption. It has been seen, however, that the behavior of line $C1$ under uniaxial stress is quite different from that either of the A or B lines. It is possible that this is due to differences in the nature of the ground states in the two cases. It should also be noted that the low-energy counterpart of $A1$ and $B1$ has not been observed in the C spectrum. Line $D1$ is somewhat unique in that it appears to be the only line associated with the D center, and in that its behavior under uniaxial stress differs from that of the other strong lines.

By treating acceptors in AlSb on the basis of a T_d site symmetry and valence-band maximum at $\mathbf{k}=0$, it has been possible to account for most of the observed piezospectroscopic effects. It is perhaps surprising, in view of the complicated theoretical valence-band structure for AlSb, that the behavior of $A1$, $A2$, $A3$, $D1$, and $B2$ under uniaxial stress has been interpreted as successfully as it has been in terms of a germaniumlike valence band. The success of this model may perhaps be understood to some extent by comparing the spread in $|\mathbf{k}|$ values for a bound hole with the expected displacement of the valence-band maxima away from $\mathbf{k}=0$ in AlSb. If the spread in $|\mathbf{k}|$ values for a given state is much smaller than the shift of the valence-band maxima away from $\mathbf{k}=0$, a bound hole in this state can

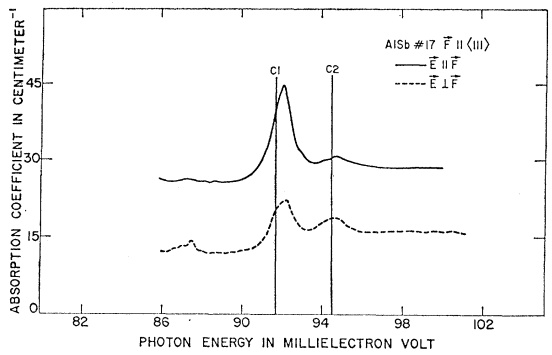

FIG. 16. Behavior of the C lines for $\mathbf{F}\|\langle 111\rangle$; $p(300°\text{K}) \approx 5\times 10^{16}$ cm^{-3}. Liquid helium used as coolant. Zero-stress positions are denoted by solid vertical lines.

be localized in k space near a particular valence-band maximum. The spectra might then be expected to show effects associated with the multiple-maxima valence-band structure. The spread in $|\mathbf{k}|$ values for bound holes due to their localization may be estimated using simple hydrogenic wave functions with Bohr orbits chosen to correspond to an ionization energy of 34 meV, which is close to that for the A and B spectra. Such calculations indicate that the spread in $|\mathbf{k}|$ values for the ground state and the first few excited bound hole states should be greater than the shifts of the valence-band maxima away from $\mathbf{k}=0$ as estimated for AlSb following Kane's valence-band calculation for InSb.[23] Hence the range of $|\mathbf{k}|$ values for holes in the more tightly bound states will overlap all of the extrema of the valence band edge in k space. The resulting superposition of the effects associated with all these closely spaced extrema might be expected to resemble those for a single broad maximum at $\mathbf{k}=0$. On the other hand, the spread in $|\mathbf{k}|$ values for the higher excited states becomes progressively smaller, so that a hole in a highly excited state might be localized at a particular maximum in k space; however, this does not appear to be the case for the lines examined.

In addition to a theoretical treatment of acceptor-state energies in AlSb, advances in the technology of

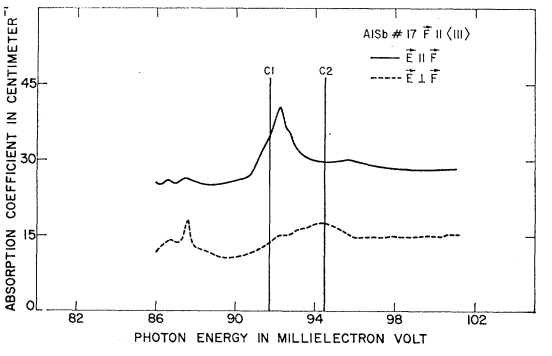

FIG. 17. Behavior of the C lines for $\mathbf{F}\|\langle 111\rangle$. The stress here is greater than that of Fig. 16. Zero-stress positions are denoted by solid vertical lines. Liquid helium used as coolant.

TABLE II. Mass-spectrographic analysis of aluminum antimonide samples.

Element	No. of atoms (cm^{-3}) Ingot 48	Ingot 52[a]
Na	3.36×10^{17}	1.12×10^{17}
P	8.22×10^{15}	8.22×10^{16}
S	3.24×10^{17}	$\leq1.62\times10^{17}$
Cl	4.43×10^{17}	1.48×10^{16}
K	1.99×10^{16}	6.60×10^{16}
Ca	1.29×10^{16}	1.29×10^{16}
Cr	9.90×10^{15}	3.48×10^{15}
Mn	3.28×10^{15}	3.28×10^{16}
Fe	9.20×10^{15}	1.84×10^{15}
Co	$\leq1.31\times10^{15}$	$<1.31\times10^{15}$
Ni	4.37×10^{15}	$\leq2.19\times10^{15}$
As	1.72×10^{15}	1.03×10^{16}
Ta	$\leq1.42\times10^{16}$	$<1.42\times10^{16}$

[a] Ingots 48 and 52 are the designations given by Bell & Howell to the ingots having room-temperature hole concentrations $\approx3\times10^{15}$ cm^{-3} and 3×10^{16} cm^{-3}, respectively.

growing high-purity material are clearly necessary if further progress is to be made in the study of these states. Mass-spectrographic analyses[32] performed on AlSb crystals used in the present studies, which on the basis of hole concentration and mobility were among the purest samples ever grown, have revealed the presence of several types of foreign atoms, each in more than enough numbers to give rise to the observed spectra. The impurities detected are listed in Table II. In addition, many other impurities may be present in numbers sufficiently large to be observed optically but not large enough to be identified by the mass-spectrographic analysis. Nor has it been ruled out that one or more of these spectra is associated with nonstoichiometry. Along this line, it would be of definite interest to investigate if any of the observed lines can be produced by irradiating pure AlSb with high-energy particles. Of course, the most definitive experiment possible would be the investigation of the spectrum arising from the controlled introduction of specific group-II acceptors into AlSb.

It appears possible on the basis of the behavior of line $D1$, the weak line $A3$, and line $C1$ for $\mathbf{F}\|\langle111\rangle$, that the deformation potential constant d' for the ground state of the acceptors giving rise to these lines may be of opposite sign to that observed for group-III acceptors in silicon and germanium.[9,30] In silicon and germanium b' and d' for a bound hole state are intimately related to b and d for the valence band.[26] It is therefore interesting to note that Cardona, Laude, and Pollak[33] have determined that the signs of b and d in AlSb are the same as in silicon,[34] germanium,[35] and other III-V compounds.[35,36]

Finally, it is interesting to note that the intensities of hole photoexcitation plus phonon emission lines appear to be much smaller than was observed for the donor photoexcitation plus phonon emission lines.[10] As was noted in Ref. 10, the relative intensities of an electronic excitation line and a line arising from the same electronic transition accompanied by the simultaneous emission of a phonon, depend on the ground-state binding energy. Hence for the shallow acceptors which give rise to the A and B lines, in particular, the excitation plus phonon lines would be rather weak, as is certainly the case. A quantitative description of such transitions for the acceptor spectra remains to be given.

ACKNOWLEDGMENTS

The authors wish to thank Professor P. Fisher for many valuable discussions. They are also indebted to Professor R. J. Sladek and Professor W. M. Becker for generously supplying several of the samples used in the present investigation, and Professor H. J. Yearian for orienting the samples.

[32] The mass-spectrographic analyses were performed by the Analytical Chemistry and Spectroscopy Division, Battelle Memorial Institute, 505 King Avenue, Columbus, Ohio 43201.

[33] Manual Cardona, D. Laude, and F. H. Pollak, Bull. Am. Phys. Soc. **14**, 428 (1969).

[34] J. C. Hensel and G. Feher, Phys. Rev. **129**, 1041 (1963).

[35] Fred H. Pollak and Manual Cardona, Phys. Rev. **172**, 816 (1968).

[36] I. Balslev, J. Phys. Soc. Japan Suppl. **21**, 101 (1966); C. Benoit a la Guillaume, and P. Lavallard, *ibid.* **21**, 288 (1966).